

Article

Marangoni Convection of Dust Particles in the Boundary Layer of Maxwell Nanofluids with Varying Surface Tension and Viscosity

Khaled S. AlQdah ¹, Naseer M. Khan ² , Habib Ben Bacha ³, Jae-Dong Chung ^{4,*}  and Nehad Ali Shah ^{4,5}

¹ Mechanical Engineering Department, College of Engineering, Taibah University, Medina 42353, Saudi Arabia; dr.khaled_qdah@yahoo.com

² School of Mathematics and Statistics, Central South University, Changsha 410083, China; nmkhan@math.qau.edu.pk

³ Mechanical Engineering Department, College of Engineering at Alkharj, Prince Sattam bin Abdul-Aziz University, P.O. Box 655, Alkharj 11942, Saudi Arabia; h.benbacha@psau.edu.sa

⁴ Department of Mechanical Engineering, Sejong University, Seoul 05006, Korea; nehadali199@yahoo.com

⁵ Department of Mathematics, Lahore Leads University, Lahore 54000, Pakistan

* Correspondence: jdchung@sejong.ac.kr

Abstract: The flow of nanofluids is very important in industrial refrigeration systems. The operation of nuclear reactors and the cooling of the entire installation to improve safety and economics are entirely dependent on the application of nanofluids in water. Therefore, a model of Maxwell's dusty nanofluid with temperature-dependent viscosity, surface suction and variable surface tension under the action of solar radiation is established. The basic equations of momentum and temperature of the dust and liquid phases are solved numerically using the MATLAB bvp4c scheme. In the current evaluation, taking into account variable surface tension and varying viscosity, the effect of dust particles is studied by immersing dust particles in a nanofluid. Qualitative and quantitative discussions are provided to focus on the effect of physical parameters on mass and heat transfer. The propagation results show that this mixing effect can significantly increase the thermal conductivity of nanofluids. With small changes in the surface tension parameters, a stronger drop in the temperature distribution is observed. The suction can significantly reduce the temperature distribution of the liquid and dust phases. The stretchability of the sheet is more conducive to temperature rise. The tables are used to explain how physical parameters affect the Nusselt number and mass transfer. The increased interaction of the liquid with nanoparticles or dust particles is intended to improve the Nusselt number. This model contains features that have not been previously studied, which stimulates demand for this model among all walks of life now and in the future.

Keywords: Maxwell nanofluid; dynamics of dust particles; variable viscosity and surface tension; Marangoni convection; numerical solutions



Citation: AlQdah, K.S.; Khan, N.M.; Bacha, H.B.; Chung, J.D.; Shah, N.A. Marangoni Convection of Dust Particles in the Boundary Layer of Maxwell Nanofluids with Varying Surface Tension and Viscosity. *Coatings* **2021**, *11*, 1072. <https://doi.org/10.3390/coatings11091072>

Academic Editor: Rahmat Ellahi

Received: 26 July 2021

Accepted: 30 August 2021

Published: 5 September 2021

Publisher's Note: MDPI stays neutral with regard to jurisdictional claims in published maps and institutional affiliations.



Copyright: © 2021 by the authors. Licensee MDPI, Basel, Switzerland. This article is an open access article distributed under the terms and conditions of the Creative Commons Attribution (CC BY) license (<https://creativecommons.org/licenses/by/4.0/>).

1. Introduction

Energy drives a general world. Given its basic importance, energy security is a major issue standing up to the present reality. This is a quick result of a more noteworthy reliance on unsustainable fuel sources such as oil and gas. At the point when used, these assets cannot be restored: this creates a security issue for energy assets. To solve this serious issue, the world must move to judicious clean energy that guarantees practical transformation. Solar energy is one such asset. It is harmless to the ecosystem and endless, supplying the Earth with radiation at an obscure time. Considering these qualities, the current culture is more disposed to obtain the energy of sunlight. Solar radiation obtained by the Earth is equivalent to the possible energy of 6000 GWh every year. A large part of the time, effectiveness exceeds human interest. Consequently, the benefits of solar energy are very reasonable. While the basic cost of making it might be high, it is the most appropriate

solution given its general characteristics, sustainability, and effectiveness. Previously, individuals used the its achievements to assemble scattered light, sunlight energy, and heat.

Nanoparticles are the supported wellspring of clean energy. The size of nanoparticles goes from 1 nm to 100 nm; that is, their size is comparable to the de Broglie wavelength. Due to their small size, nanoparticles can thoroughly ingest the light energy they enter. The uniform and irregular movement of nanoparticles (Brownian movement) is expected to increase the base fluid with enormous thermal conductivity. It can be seen that the temperature development and the reduction in particle size increase the irregular movement of nanoparticles, which enables nanofluids to conduct more and more heat. Due to the radiation properties and the irregular movement of nanoparticles (Brownian movement), the use of nanofluids in the solar system offers a further test to control inputs. The viscosity of the Maxwell fluid model is independent of the shear rate, so a quadratic equation is generated at the position of the Poiseuille fluid flow field. The boundary layer approximation is more appropriate for this model than for other models. The results of the Maxwell fluid model are interesting and are of vital importance in industries [1]. Therefore, this model should be used to study the physical aspects of nanofluids. Jamshed [2] and Fetecau [3] proposed a model of a Maxwellian nanofluid moving along a stretched sheet under the action of solar radiations, and investigated the effects of various physical aspects on heat and mass transfer.

In recent decades, the nanofluid has been widely addressed by researchers due to its improvement in thermal conductivity [4–7]. The Brownian movement of nanoparticles is the only way to help improve the thermal conductivity of the nanofluid. Since they are widely used in many industrial and technical processes, many researchers have studied the physical aspects of nanofluid under different physical conditions. The sheet stretching properties affect the physical properties of the nanofluid, so the mass and heat transfer analysis of MHD nanofluids on the stretching sheet are new learning access points for many researchers. Nanofluid does not have to be purified. The addition of dust particles in the nanofluid suspension is more likely to affect the physical properties of the nanofluid. However, the investigation of dusty nanofluid needs more attention than other nanofluids that are no longer studied. This analysis focuses on the mass and heat transport of nanofluid suspensions that contain dust particles. The volume fractions of dust particles and nanofluids are measured in nm and μm while developing a flow model. Due to the improved thermal conductivity of nanofluids, they are used in electronic devices as a coolant, as energy cartridges in companies and automobiles, in optical devices, and in micromechanical devices. Because of their high demand, in almost all spheres of life, the study of nanofluid has developed significantly in recent decades.

Siddiqua [8] is one of those who pioneered the idea of a laminar boundary flow of gases saturated with dust particles. Hamilton [9] proposed a model that demonstrates aspects of thermal conductivity in the boundary layer of a system with two components. Day [10] discussed several physical aspects of dusty bioconvective nanofluids under various circumstances. Zhang [11] and Ijaz [12] took the initiative to investigate the mass and heat transport of an MHD fluid moving across a stretched sheet. Krishna [13] revealed the influence of various physical aspects on the mass and heat transport of a fluid (second grade) through theoretical approaches. Yun-Xiang Li [14] conducted research to study various physical aspects of Maxwell's unsteady nanofluid flowing through a stretched sheet. Mohammadein [15] designed a mathematical model to discuss the effects of various parameters on the mass and heat transfer of MHD nanofluids, including suction conditions and flow over the stretched surface. Taking into account the influence of porosity, Zainal [16] undertook an initiative to investigate the properties of MHD fluid flowing through a vertical flat plate. Eastman [17] first visualized the concept that the suspension of nanoparticles has a higher thermal conductivity than the base liquid. Sandeep [18] studied heat and mass transfer in the boundary layer of dusty MHD nanofluids. Dusty nanofluid can be thought of as a combination of dust particles and nanofluid. A mixed convective

boundary layer flow of fluids was investigated by Ishak [19] in order to discuss the effects of various physical aspects on the transport of mass and heat.

Of course, MHD or magnetohydrodynamics is a conductive fluid that passes through a magnetic field and can be used to study the influence of a magnetic field on a fluid stream. The fundamental improvement of MHD for the most part lies in the dynamo theory, which describes how the advancement of fluids inside stars and planets creates and maintains a worldwide magnetic field. MHD stream is for the most part used in numerous industries and designing technologies such as refineries, plasma analysis, and the chemical industry. Ghosh [20] studied the dusty MHD Maxwell fluid on a rectangular surface and discussed many of its thermophysical properties. Ahmed [21] studied the influence of various physical aspects on the mass and heat transport of a dusty fluid flow on a Frenet frame. Damseh [22] drove a study to discuss the characteristics of the stream in the boundary layer influenced by a magnetic field coursing through an exponentially stretched sheet. Sandeep [23] designed a study to investigate various physical aspects of a dusty MHD fluid flowing over a stretched surface. Bhattacharyya [24] finished an investigation of the MHD boundary layer flow and discussed various aspects that are caused by the implanted magnetic fields. Allan proposed a mathematical model to study the behavior of a dusty gas flowing over a medium that is naturally porous. R. Ellahi [25] believed that the shape of particles affects the physical properties of alumina nanofluids, which they uncovered with the help of a mathematical model. The effects of MHD on a convective flow in the boundary layer of a dusty fluid was examined by Saidu [26]. Noreen [27] developed a model of a tangential hyperbolic nanofluid to investigate the influence of MHD on the convective flow in the boundary layer. Therefore, the MHD stream is welcomed by researchers because of its wide application in numerous industries and designing technologies. In this article we have included many recent studies to describe the effect of MHD on mass and heat transfer.

Wahid [28] used the Marangoni flow model to study the influence of suction on mass and heat transport in the nanofluid boundary layer. Hossain [29] analyzed the influence of natural convection on a laminar unsteady fluid moving along a vertical perforated plate in a porous medium. Considering the natural convective flow over an infinite vertical flat plate, Sandeep [30] developed a mathematical model to analyze the influence of thermal radiations on the heat and mass transfer of nanofluids. Considering the natural convective flow of an unsteady MHD nanofluid over an infinite vertical flat plate, Mandal [31] developed a mathematical model to visualize the influence of solar radiation on the characteristics of mass and heat transfer. Later, Daniel [32] studied the influence of chemical reactions, radiation and magnetic fields on the mass and heat transport of dusty nanofluids flowing through a heat-conducting medium. Taking viscous dissipation into account, Ghasemi [33] studied the effect of various physical parameters on the transfer of mass and energy in the boundary layer of a nanofluid flowing through a stretched sheet.

Previous research has mainly focused on dusty nanofluids with temperature-independent viscosity and surface tension. For example, Sandeep [34] and many other researchers have studied dusty nanofluids by looking at surface tension and viscosity regardless of temperature. Compared to the temperature-independent viscosity of dusty nanofluids, the temperature-dependent viscosity requires more attention and has not been further investigated. As far as we know, the current research focuses on the mass and energy transport of dusty nanofluids with temperature-dependent viscosity and surface tension. This is a new learning entry point that has never been discussed before. The results presented by this particular system reflect many new applications in various industrial and engineering applications such as manufacturing processes, artificial fibers, plastic foam processing, polymer applications, extrusion systems, heat transfer enhancement, solar energy applications, etc. The numerical tool “bvp4c” that can be run in MATLAB is used to track the numerical solution of the current problem. The results were analyzed using graphs and tables, and quantitative discussions were conducted.

2. Mathematical Modeling

The laminar boundary layer flow of the dusty Maxwell nanofluid is projected into the XY plane in combination with the surface suction, moving along the stretching sheet. In the current flow model, it is assumed that both the surface tension and the viscosity of the nanofluid are temperature-dependent (see Figure 1). The porous sheet is placed in the direction pointing to the positive x coordinate, and the dusty nanofluid flow is directed to the region where $y > 0$. A magnetic field of constant intensity $B = (0, B_0, 0)$ is introduced in the direction perpendicular to the sheet. It is believed that the results of induced magnetic and electric fields (generated by charge polarization or external magnetic fields) do not interfere with the flow of fluid. Readers may refer to [35] for a more in-depth study of induced electric and magnetic fields. When developing the flow model, the numerical density and the volume fraction of nanoscale spherical dust particles as well as the volume fraction of nanoparticles were taken into account. The velocity components of nanofluid and dust particles are represented as (u, v) and (u_p, v_p) , respectively, and temperatures are represented as T and T_p . The introduction of the boundary layer approximation in combination with the above assumptions helps in developing the prevailing equations for both the dust phase and nanofluid as:

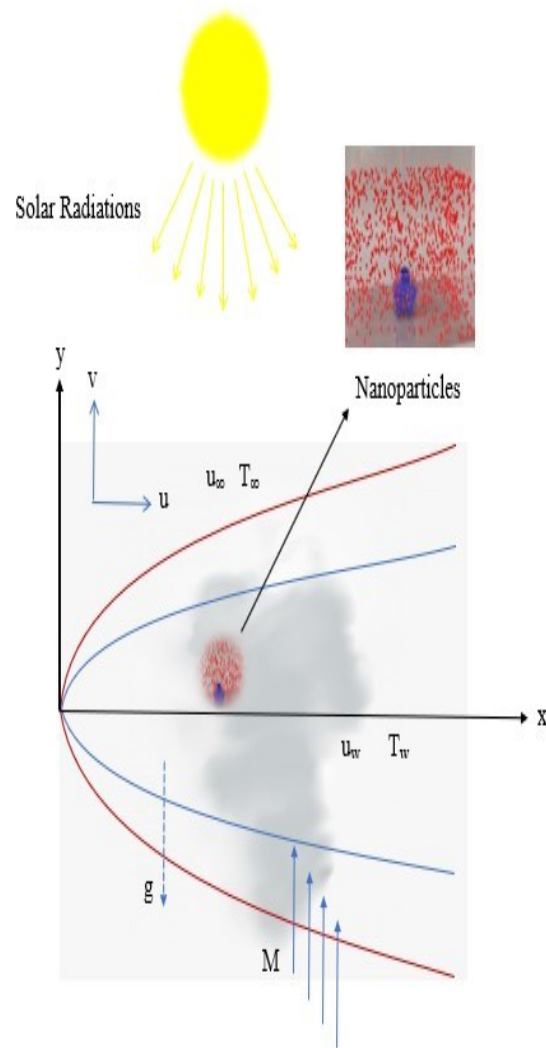


Figure 1. Flow analysis.

$$\frac{\partial u}{\partial x} + \frac{\partial v}{\partial y} = 0, \quad (1)$$

$$u \frac{\partial u}{\partial x} + v \frac{\partial u}{\partial y} = \frac{\mu_{nf}}{\rho_{nf}} \frac{\partial^2 u}{\partial y^2} + \frac{\partial \mu_{nf}}{\partial T} \frac{\partial T}{\partial y} \frac{\partial u}{\partial y} + \frac{KN}{\rho_{nf}(1-\phi_d)} (u_p - u) - \frac{\sigma B_0^2}{\rho_{nf}(1-\phi_d)} u - \frac{\mu_f}{k_1 \rho_{nf}(1-\phi_d)} u, \quad (2)$$

$$u \frac{\partial T}{\partial x} + v \frac{\partial T}{\partial y} = \frac{k_{nf}}{(\rho c_p)_{nf}} \frac{\partial^2 T}{\partial y^2} + \frac{N_1(c_p)_f}{\tau_T(\rho c_p)_{nf}} (T_p - T) - \frac{1}{\rho(c_p)_{nf}} \frac{\partial q_r}{\partial y} + \frac{N_1}{\tau_v(\rho c_p)_{nf}} (u_p - u)^2, \quad (3)$$

$$\frac{\partial u_p}{\partial x} + \frac{\partial v_p}{\partial y} = 0, \quad (4)$$

$$u_p \frac{\partial u_p}{\partial x} + v_p \frac{\partial u_p}{\partial y} = \frac{K}{m} (u - u_p), \quad (5)$$

$$u_p \frac{\partial T_p}{\partial x} + v_p \frac{\partial T_p}{\partial y} = \frac{N(c_p)_{nf}}{\tau_T N_1 c_m} (T_p - T). \quad (6)$$

The boundary conditions are embedded as:

$$\left. \begin{aligned} \mu_{nf} \frac{\partial u}{\partial y} = \frac{d\sigma}{dT} \frac{dT}{dx}, v = v_0, T = T_w = t_\infty + Ax^2 \text{ at } y = 0, \\ u \rightarrow 0, u_p \rightarrow 0, v_p \rightarrow v, T \rightarrow T_\infty, T_p \rightarrow T_\infty \text{ as } y \rightarrow \infty \end{aligned} \right\} \quad (7)$$

The flow problem is based on physical parameters. It is necessary to deal with the relevant parameters of the flow model in order to understand the flow model. First, let us describe the parameters associated with the flow model. The σ occurring in the boundary conditions denotes the temperature-dependent viscosity, and T_w and T_∞ denote the temperature of the wall and the free stream. The rest of the parameters are described in the nomenclature table at the end. Readers may refer to previous publications [36,37] for an in-depth study of energy and concentration equations.

The viscosity of the nanofluid is highly dependent on temperature and, according to previous publications [38], it can be considered as:

$$\mu = \mu^* \{a + b(T_w - T)\}, \quad (8)$$

μ^* , a , and b are all constants, μ^* represents the free stream viscosity index, and $b > 0$. Equation (8) is very similar to the equation $\mu = \mu_\infty \{1 + \gamma(T - T_\infty)\}$ obtained by Ling [39] for viscous fluids, where μ_∞ is the viscosity index of the ambient fluid and γ is a constant representing the thermal characteristics of the fluid. The flow model has been studied at near room temperature, that is, in the temperature range of 0 to 25 °C.

In a similar way, the surface tension is strongly temperature dependent and according to earlier publications [40] can be considered as follows:

$$\sigma = \sigma_0 [1 - \gamma_T(T - T_\infty)], \quad (9)$$

where σ_0 is the surface tension of the free flow and $\gamma_T (> 0)$ represents the thermal properties of the dusty nanofluid. The radiant heat q_r can be expressed with the help of famous approximations of Rosseland as:

$$q_r = -4 \frac{\sigma_1}{3k^*} \frac{\partial T^4}{\partial y}, \quad (10)$$

where the parameters k^* and σ_1 refer to absorption and Stefan Boltzmann constants. To linearize T^4 appearing in Equation (10), a Taylor series centered on T_∞ can be used to extend T^4 , assuming that the difference $T - T_\infty$ is very small.

$$T^4 = T_\infty^4 + 4T_\infty^3(T - T_\infty) + 6T_\infty^2(T - T_\infty)^2 + \dots \quad (11)$$

Ignoring the second and higher powers of $T - T_\infty$, we can write:

$$T^4 \cong 4TT_\infty^3 - 3T_\infty^4. \quad (12)$$

The radiant heat flux can be written as:

$$q_r = \frac{-4\sigma_1}{3k^*} 4T_\infty^3 T_y = \frac{-16\sigma_1 T_\infty^3}{3k^*} T_y. \quad (13)$$

Equations (2) and (3) take shape after substitution of the temperature-dependent viscosity and the value of the radiant heat flux.

$$\begin{aligned} \rho_{nf}(1 - \phi_d) \left(u \frac{\partial u}{\partial x} + v \frac{\partial u}{\partial y} \right) = & \mu^*(1 - \phi_d) (a + \xi(1 - \theta)) \frac{\partial^2 u}{\partial y^2} + KN(u_p - u) + \frac{\partial \mu}{\partial T} \frac{\partial T}{\partial y} \frac{\partial u}{\partial y} \\ & - \sigma(B_0)^2 u - \frac{\mu_f}{k_1} u, \end{aligned} \quad (14)$$

$$\begin{aligned} u \frac{\partial T}{\partial x} + v \frac{\partial T}{\partial y} = & \frac{k_{nf}}{(\rho c_p)_{nf}} \frac{\partial^2 T}{\partial y^2} + \frac{1}{\rho(c_p)_{nf}} \frac{16\sigma T_\infty^3}{3k^*} \frac{\partial^2 T}{\partial y^2} + \frac{N_1(c_p)_{nf}}{\tau_T(\rho c_p)_{nf}} (T_p - T) \\ & + \frac{N_1}{\tau_v(\rho c_p)_{nf}} (u_p - u)^2. \end{aligned} \quad (15)$$

We introduce the similarity variables as:

$$\left. \begin{aligned} u = (cx) \frac{\partial f}{\partial \eta}, v = - \left(cv_f \right)^{\frac{1}{2}} f(\eta), \eta = \left(\frac{c}{v_f} \right)^{\frac{1}{2}} y, \theta = \frac{T - T_\infty}{T_w - T_\infty}, \\ \text{where } T - T_\infty = A \left(\frac{x}{y} \right)^2 \theta(\eta) \text{ with } A > 0, \\ u_p = (cx) \frac{\partial F}{\partial \eta}, v_p = - \left(cv_f \right)^{\frac{1}{2}} F(\eta), \theta_p = \frac{T_p - T_\infty}{T_w - T_\infty}. \end{aligned} \right\} \quad (16)$$

The continuity equations are identically satisfied and the system of Equations (2), (3), (5) and (6) yields the non dimensional form of momentum, energy and concentration equations after introducing the above similarity variables.

$$\begin{aligned} \mu_1(1 - \phi_d)[a + \zeta(1 - \theta)]f''' - \left[1 - \phi + \phi \frac{(\rho)_s}{(\rho)_f}\right](1 - \phi_d)(f'^2 - ff'') \\ + \alpha\beta(F' - f') - (M + K_1)f' - \mu_1\zeta f''\theta' = 0, \end{aligned} \quad (17)$$

$$(F')^2 - FF'' + \beta(F' - f') = 0, \quad (18)$$

$$\begin{aligned} \frac{1}{Pr} \left[\frac{\frac{k_{nf}}{k_f}}{1 - \phi + \phi \frac{(\rho c_p)_s}{(\rho c_p)_f}} + Rd \right] \theta'' - (2f'\theta - f\theta') + \alpha\beta_T \left[\frac{1}{1 - \phi + \phi \frac{(\rho c_p)_s}{(\rho c_p)_f}} \right] (\theta_p - \theta) \\ + \alpha Ec \left[\frac{1}{1 - \phi + \phi \frac{(\rho c_p)_s}{(\rho c_p)_f}} \right] (F' - f')^2 = 0 \end{aligned} \quad (19)$$

$$2F'\theta_p - F\theta_p' + \gamma\beta_T(\theta_p - \theta) = 0 \quad (20)$$

The associated boundary conditions are

$$\left. \begin{aligned} f''(\eta) = -\delta, f(\eta) = s, \theta(\eta) = 1 \text{ at } \eta = 0, \\ f'(\eta) \rightarrow 0, F'(\eta) \rightarrow 0, F(\eta) = f(\eta), \theta(\eta) \rightarrow 0, \theta_p(\eta) \rightarrow 0 \text{ as } \eta \rightarrow \infty. \end{aligned} \right\} \quad (21)$$

The physical aspects of nanofluids are given by:

$$\left. \begin{aligned} \frac{(\rho c_p)_{nf}}{(\rho c_p)_f} &= (1 - \phi) + \phi \frac{(\rho c_p)_s}{(\rho c_p)_f}, \frac{\mu_{nf}}{\mu_f} = 1 + k_\mu \phi \text{ where } k_\mu = 2.5, \\ \frac{k_{nf}}{k_f} &= [k_s + 2k_f - 2\phi(k_f - k_s)] [k_s + 2k_f + \phi(k_f - k_s)]^{-1}, \\ \frac{\rho_{nf}}{\rho_f} &= 1 + \left(\frac{\rho_s}{\rho_f} - 1\right)\phi. \end{aligned} \right\} \quad (22)$$

where ρ_{nf} and ρ_f correspond to the density of the nanofluid and the base fluid. μ_{nf} and μ_f represent the viscosity of the nanofluid and the base fluid, respectively. $c_{p_{nf}}$ and c_{p_f} are the specific heat capacity of the nanofluid and the base fluid, while the volumetric ratio of the nanoparticle to that of the base fluid is represented by ϕ . $\zeta = b(T_w - T_\infty)$, where b is a dimensionless constant. The ratio of the freestream viscosity to the base fluid viscosity is represented as $\mu_1 = \frac{\mu^*}{\mu_f}$. $\alpha = \frac{Nm}{\rho_f}$ and $\beta = \frac{K}{c_m}$, respectively, refer to the mass concentration of dust particles and the parameter of the velocity interaction of liquid particles. The porosity parameter and Prandtl number are, respectively, expressed as $K_1 = \frac{v_f}{ck_1}$ and $Pr = \frac{v_f}{\alpha_f}$. $l = \sqrt{v_f/c} > 0$ refers to the characteristic length, $\beta_T = \frac{1}{c\tau_T}$ refers to the temperature interaction parameter of fluid particles, $Ec = \frac{cl^2}{A(c_p)_f}$ refers to the Eckert number. $\gamma = \frac{(c_p)_f}{c_m}$ corresponds to the ratio of the specific heat of the fluid to the dust particles.

Heat is transferred from one place to another in three different ways: conduction, convection, and radiation. The terms conductivity (diffusion) and advection (fluid movement) are collectively referred to as convection. The ratio of heat conduction to convection at a particular boundary is named the Nusselt number after William Nusselt, who made a significant contribution to heat transfer, especially convective heat transfer. Assuming the fluid is at rest, heat transfer can be measured under the same conditions as convective

heat transfer. The Nusselt number measures net thermal conductivity. Laminar flow is characterized by a Nusselt number from 1 to 10, and a turbulent flow is characterized by a Nusselt number from 100 to 1000. Both conduction and convection heat transfer are perpendicular to the boundary surface and parallel to each other.

The Nusselt number in terms of heat transfer coefficient h_{nf} and a characteristic length l is given by the formula

$$\text{Nusselt number} = \frac{\text{Heat transfer through Convection}}{\text{Heat transfer Conduction}} = \frac{h_{nf}}{\frac{k_{nf}}{l}} = \frac{h_{nf} l}{k_{kn}}$$

In view of its important physical significance, the research on Nusselt number, skin friction coefficient and Sherwood number cannot be ignored. They are given by the formulae:

$$\left. \begin{aligned} c_{fx} &= \frac{\tau_w}{\rho_{nf}(u_w)^2} \text{ where } u_w = cx, \\ Nu_x &= \frac{xq_w}{k_{nf}(T_w - T_\infty)}, \end{aligned} \right\} \quad (23)$$

where τ_w and q_w in Equation (20) represent the shear stress and the heat flux of the wall is given by:

$$\left. \begin{aligned} \tau_w &= \mu_{nf} \frac{\partial u}{\partial y} \Big|_{y=0}, \\ q_w &= \left[-k_{nf} \frac{\partial T}{\partial y} + q_r \right]_{y=0}. \end{aligned} \right\} \quad (24)$$

By introducing the Equations (24) and (17), it is possible to achieve dimensionless values for the skin friction coefficient and the Nusselt number.

$$\left. \begin{aligned} \sqrt{Re_x} C_{fx} &= f''(0), \\ Nu_x (\sqrt{Re_x})^{-1} &= -(1 + Rd)\theta'(0). \end{aligned} \right\} \quad (25)$$

It was found that the dimensionless mass flux, namely the local Sherwood number, is zero.

3. Numerical Techniques

Through the first replacement of the similarity variables, the prevailing partial differential equations and boundary conditions are transformed into nonlinear ordinary differential equations. The resulting Equations (18)–(21) and the related boundary conditions (22) are converted into linear ordinary differential equations using appropriate variables. It is then input into a MATLAB scheme called the boundary value problem solver (abbreviated as bvp4c) to solve it. The collocation method is used to find solutions to the problems listed below:

$$y' = \Lambda(p, y), \quad g \leq t \leq h \quad (26)$$

The corresponding boundary conditions can be written as:

$$bc(y(g), y(h)) = 0. \quad (27)$$

$\zeta(p)$ is the approximate solution of the above system, which is a cubic polynomial on each subinterval $[p_j, p_{j+1}]$ of the grid $g = p_0 < p_1, \dots, p_j = h$, and meets the boundary conditions.

$$bc(\zeta(g), \zeta(h)) = 0 \quad (28)$$

Equivalently, $\zeta(p)$ satisfies the system of the ODE's (*collocates*) at both ends of each sub-interval and the midpoint.

$$\left. \begin{aligned} \zeta'(p_j) &= \Lambda(p_j, \zeta(q_j)), \\ \zeta'\left(\frac{p_j+p_{j+1}}{2}\right) &= \Lambda\left[\left(\frac{p_j+p_{j+1}}{2}\right), \zeta\left(\frac{q_j+q_{j+1}}{2}\right)\right], \\ \zeta'(p_{j+1}) &= \Lambda[p_{j+1}, \zeta(p_{j+1})]. \end{aligned} \right\} \tag{29}$$

$\zeta(p)$ is an approximate solution of the above-mentioned nonlinear algebraic equations, found by the linearization method. The solution $\zeta(p)$ to $y(p)$ is a fourth-order differential equation, namely $\|y(p) - \zeta(p)\| \leq k_1 \Lambda^4$. The constant k_1 in the above relationship represents the maximum value of $\Lambda_j = p_{j+1} - p_j$. The residual of the solution $\zeta(p)$ is represented by the equation $R(t)$, which is a differential equation defined as follows:

$$R(t) = \zeta'(q) - \Lambda(p, \zeta(p)) \tag{30}$$

When using the `bvp4c` scheme in MATLAB, error control and grid point selection should be carried out according to the residuals. The condition that η is close to infinity should be replaced by a suitable number. Here, we took $\eta = \eta_\infty = 5$. When we are looking for the most suitable solution to the problem of the Equations (18)–(21) and the corresponding boundary conditions, we take appropriate initial guesses. It is easy to find the initial guess for the first solution, but it requires a lot of computational work to find the initial guess for the second solution; therefore, we randomly select an initial guess and a set of parameters, and use the continuation technique to reach the exact value of parameters.

4. Results and Discussions

Maxwell's two-dimensional flow of dusty nanofluid was developed under the influence of solar radiation. The Upper Convected Maxwell model (UCM) was introduced to include momentum and energy equations, and the Rosseland approximations were used to explain the characteristics of thermal radiation. The nanofluid flow is assumed to move along an exponentially stretching surface. The nonlinearity of the PDE system is reduced by converting it into a coupled nonlinear ordinary differential equation and then using a numerical tool called "bvp4c" in MATLAB to solve it. The accuracy and convergence of the solutions found with "bvp4c" were checked by comparing them with already published articles [41,42] on Table 1, and found similar ones. Because of its high accuracy, excellent convergence and lower computational cost, we can argue that "bvp4c" is one of the preferred numeric tools. After the introduction of `bvp4c` to find a solution to the problem, the influence of each parameter on the speed and temperature of dusty and dustless nanofluids was studied and investigated using tables and graphs, while other parameters remained unchanged. The rest of the parameters are assigned values like $\mu^* = 0.5, \phi_d = 0.5, a = 0.5, \xi = 0.5, \phi = 0.7, \delta = 0.5, m = 0.05, \alpha = 0.5, \beta = 0.5, s = 0.5, \gamma = 0.5, \beta_T = 0.5, M = 1.5, K_1 = 0.5, Pr = 7, Ec = 0.1$, and $Rd = 0.5$.

Table 1. Comparison of the current results with already published papers.

Pr	Current Results	Mishra [41]	Mahanthesh [42]
0.72	1.088575	1.088562	1.0884
1.00	1.333348	1.333333	1.3333
10.0	4.796831	4.796819	4.7968

Figure 2a illustrates the influence of μ_1 (μ_1 is the ratio of free-flow viscosity to base fluid viscosity) on the fluid phase velocity profile represented by the solid line and the dust phase represented by the dashed line. By increasing the value of μ_1 , it makes a significant contribution to the increase in the velocity distribution of the dustless nanofluid, while the contribution of μ_1 to the stimulation of the velocity of the dusty nanofluid is insignificant. As the value of μ_1 increases, the thickness of the momentum boundary layer of dust-free

and dusty fluids increases. Figure 2b discusses the influence of ϕ_d (the ratio of the volume of nanoparticles to the total volume of the mixture) on the speed distribution of dust-free and dusty nanofluids. When increasing the value of ϕ_d , the velocity distribution of both dust-free and dusty nanofluids will decrease. When improving the value of ϕ_d , the viscous boundary layer thickens slightly, regardless of whether the nanofluid is dust-free or dusty. ϕ is the concentration of nanoparticles per unit volume, which influences the velocity profile of dust-free and dusty nanofluids, as shown in the Figure 2c. A small increase in the fractional concentration of nanomaterials can cause a significant improvement in the velocity profile. If the concentration of the nanoparticles per unit volume increases, the penetration depth of the momentum boundary layer increases.

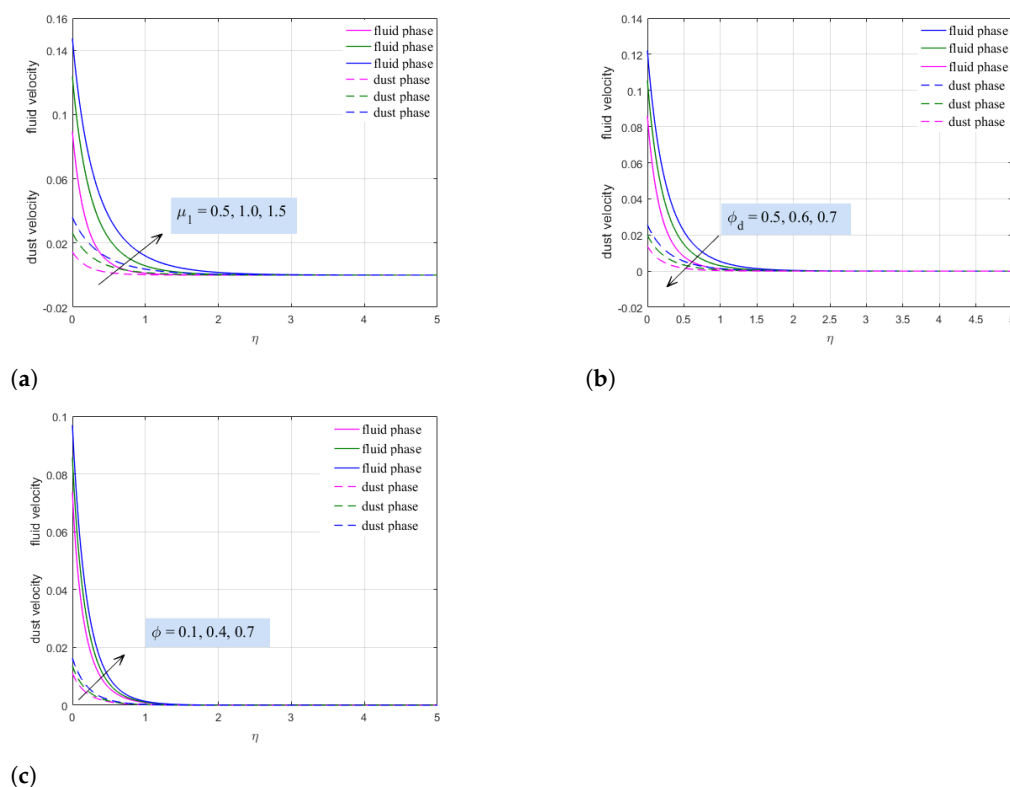
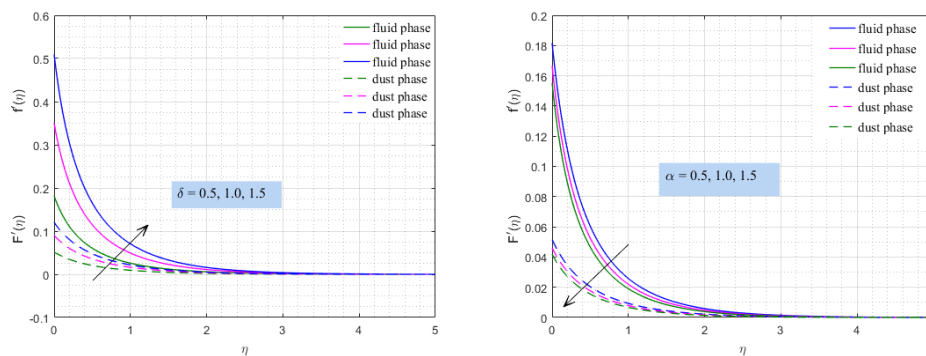


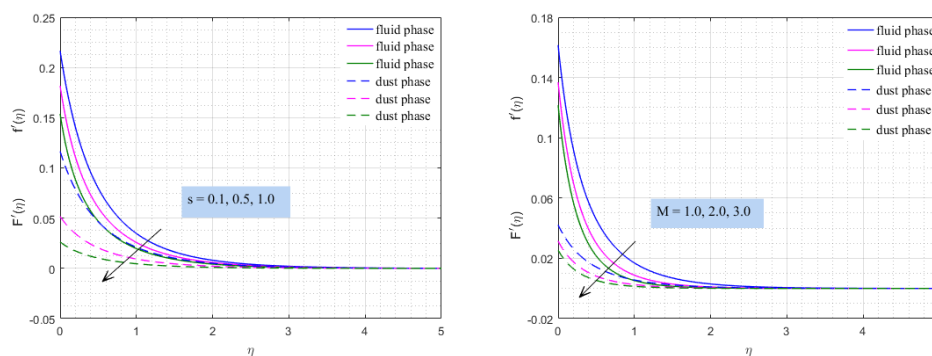
Figure 2. Velocity curves for different values of physical parameters. (a) Change in velocity at different values of μ_1 . (b) Change in velocity at different values of ϕ_d . (c) Change in velocity at different values of ϕ .

Figure 3a examines how the variable surface tension δ affects the velocity distribution of both the dust-free and the dusty nanofluid. This figure shows that increasing the values of δ increases the velocity distribution and that the viscous boundary layer becomes thicker in both cases (regardless of whether the fluid is dusty or free of dust). By increasing the mass concentration of nanoparticles α , the velocity distribution decreases as expected, as shown in Figure 3b. Moreover, α significantly increases the penetration depth of momentum in the dust-free and dusty nanofluid boundary layer. The movement of fluid from the low pressure zone to the high pressure zone is mathematically regarded as suction. The low-pressure zone is called the inlet zone, and the high-pressure zone is called the outlet zone. In such applications, the lowest pressure area needs to be selected. In this study, $\eta = 0$ is regarded as the lowest pressure zone. If liquid enters an area where the pressure is comparatively higher than the area where the liquid was, it means that the suction values are higher. It can be seen from the adjacent figure that the volume of the fluid decreases when it passes through the equilibrium zone, thereby reducing the flow rate, usually reaching a maximum. To see how the suction parameter s affects the velocity in the graph, a graph is shown in the Figure 4a. Due to the increase in the suction parameter

value, the speed of the dust and liquid phase on the graph decreases, as can be seen from the adjacent graph. In both cases, the penetration depth of the viscous boundary layer decreases as the suction parameter s becomes larger. Increasing the value of the magnetic field parameter M can significantly reduce the velocity distribution of the dust phase and the fluid phase, and the momentum boundary layer becomes thinner when increasing M , as shown in Figure 4b.



(a) (b)
Figure 3. Change in the velocity profile at different values of certain parameters. (a) Change in velocity profile at different values of δ . (b) Change in velocity profile at different values of α .



(a) (b)
Figure 4. Change in the velocity profile at different values of certain parameters. (a) Change in velocity profile at different values of s . (b) Change in velocity profile at different values of M .

Figure 5a schematically shows the effect of the surface tension parameter δ on the temperature distribution of the dust and liquid phases, which indicates that an increase in the surface tension parameter δ does not actually contribute to an increase in temperature in these two cases. The penetration depth of the temperature boundary layer is directly proportional to the change in δ . Figure 5b exhibits that the temperature distribution is significantly influenced by the volume fraction of dust particles ϕ_d . The increase in the volume fraction of dust particles contributes to the increase in temperature distribution in the fluid and dust phases. As ϕ_d increases, the temperature boundary layer becomes thicker. The Figure 5c shows that an increase in the concentration of nanoparticles will lead to an increase in the temperature profile. As the volume fraction of nanoparticles increases, the frequency of collisions between nanoparticles increases, and collisions between nanoparticles become more likely. The number of particle collisions increases as the temperature value increases, thereby increasing the kinetic energy of translation, rotation, and vibration of the nanoparticles and, as a result, the temperature of the base fluid increases. On the other hand, if we increase the temperature of the fluid containing nanoparticles, the externally provided energy will be used to increase the random motion of the nanoparticles

and, as a consequence, lower temperature profiles can be seen for increased values of the Brownian motion parameter.

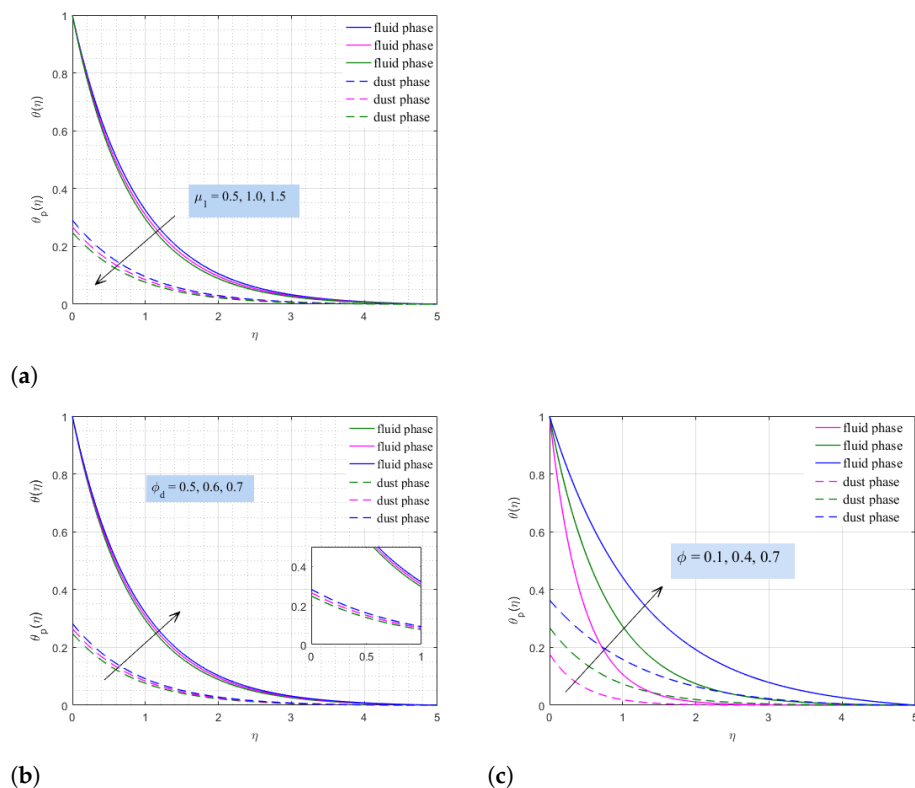


Figure 5. Concentration profiles for different values of parameters. (a) Change in temperature distribution at different μ_1 values. (b) Change in temperature distribution at different ϕ_d values. (c) Change in temperature distribution at different ϕ values.

Figure 6a discusses the influence of the surface tension parameter δ on the temperature distribution of the fluid and dust phases in the presence of solar radiation, indicating that the surface tension parameter has a significant effect on the temperature distribution and the thickness of the thermal boundary layer. With a small change in the value of the surface tension parameter, a greater decrease in the temperature distribution is observed. The thermal boundary layer decreases as δ increases. The influence of dust particles mass concentration α on temperature distribution is shown in the Figure 6b, which indicates that the increase in nanoparticles mass concentration value leads to a significant decrease in temperature distribution, and the thickness of the thermal boundary layer decreases as α increases. The influence of the suction parameter s on the temperature distribution is shown in Figure 6c. This diagram is slightly different from other structural diagrams. As the suction parameter increases, a significant decrease in the temperature distribution of the fluid and dust phases can be observed at lower values of η , and a slight drop can be observed at larger values of η . As the surface suction s increases, the thickness of the thermal boundary layer decreases. Figure 6d illustrates the influence of the magnetic field parameter M on the temperature distribution, indicating that the temperature distribution increases slightly with the increase in the magnetic field parameter. The increase in the magnetic field parameter M results in the thickening of the temperature boundary layer.

Table 2 examines the effects of various parameters on skin friction and heat transfer rate. It can be observed that the heat transfer rate increases as the values of μ_1 , ϕ , δ , α , and s increase, while the skin friction remains the same, but decreases as δ increases. The heat transfer rate decreases with increasing volume fraction of dust particles ϕ_d and magnetic field parameters M and skin friction remain unchanged when they are increased.

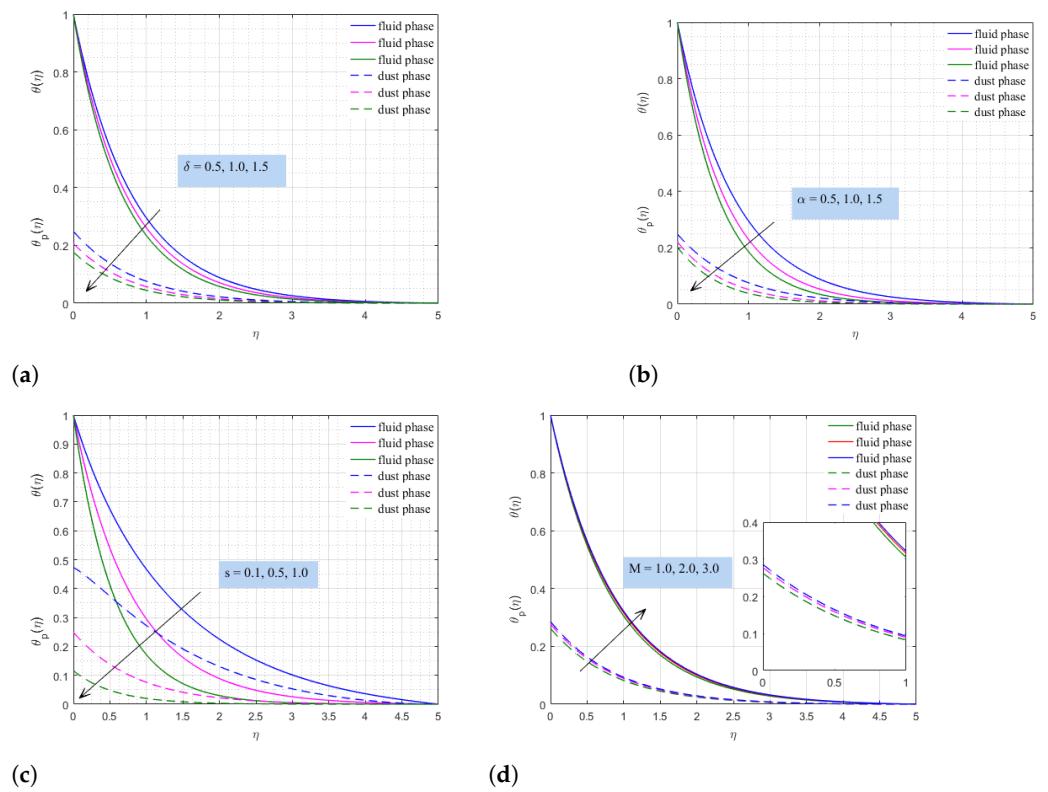


Figure 6. Change in concentration curves for different values of certain parameters. (a) Change in temperature profile at different δ values. (b) Change in temperature profile at different α values. (c) Change in temperature profile at different s values. (d) Change in temperature profile at different M values.

Table 2. Change in the coefficient of surface friction C_{f_x} and Nusselt number Nu_x at different values of certain physical parameters.

μ_1	ϕ_d	ϕ	δ	α	s	M	$f''(0)$	$-\theta'(0)$
0.5							-0.5000	1.7312
1.0							-0.5000	1.8261
1.5							-0.5000	1.8999
	0.5						-0.5000	1.7312
	0.6						-0.5000	1.7048
	0.7						-0.5000	1.6774
		0.5					-0.5000	1.7312
		1.0					-0.5000	0.80908
		1.5					-0.5000	0.35507
			0.5				-0.5000	1.7312
			1.0				-1.0000	1.8443
			1.5				-1.5000	1.9497
				0.5			-0.5000	1.7312
				1.0			-0.5000	2.1256
				1.5			-0.5000	2.4530
					0.5		-0.5000	0.93695
					1.0		-0.5000	1.7312
					1.5		-0.5000	2.5361
						0.5	-0.5000	1.7312
						1.0	-0.5000	1.7066
						1.5	-0.5000	1.6908

5. Conclusions

Considering the temperature-dependent viscosity, surface suction and variable surface tension, a Maxwell dusty nanofluid model under the action of solar radiation is established. The basic equations of momentum and temperature of the dusty and fluid phases are numerically solved using the MATLAB bvp4c scheme. In the boundary layer flow of Maxwell's dusty nanofluid model, the physical aspects of several parameters are studied, and graphs and tables are used for analysis and quantitative discussion. The conclusion is that the microconvection generated by the Brownian motion of the nanoparticles can increase the thermal conductivity of the base fluid. Due to the hydrodynamic connection between Brownian motion nanoparticles, this information combined with various studies on the viscosity of nanofluids is very convincing [43–48].

- The results undeniably demonstrate the microconvection effects achieved by the Brownian motion of nanoparticles in these suspensions, and show that high concentrations of nanoparticles help to convincingly increase the thermal conductivity of the base fluid.
- α , the mass concentration of dust particles, significantly improves the thermal conductivity of the nanofluid.
- The cooling rate in an industrial refrigeration system can be adjusted by increasing/decreasing surface suction.
- The parameter μ_1 generated by the temperature-dependent viscosity has a strong influence on the temperature profile, which indicates that this parameter tends to reduce the thermal conductivity of the base fluid.
- The variable surface tension parameter δ will destroy the thermal conductivity of the dusty nanofluid, and the thermal conductivity can be improved by enhancing the implanted magnetic field.
- An increase in the density of nanoparticles is inductive with an increase in the temperature distribution, but opposite to the velocity distribution. The same applies to the density of the dust particles.
- The increased interaction of the liquid with nanoparticles or dust particles is intended to improve the Nusselt number.

Author Contributions: Oversight and leadership responsibility for the research activity planning and execution, including mentorship external to the core team, K.S.A. and N.A.S.; Presented the idea for this study, mathematical formulation, tabular and graphical results, qualitative and quantitative discussion, N.M.K.; Conducting a research and investigation process, specifically performing the experiments, or data/evidence collection, H.B.B. Acquisition of the financial support for the project leading to this publication, J.-D.C. All authors have read and agreed to the published version of the manuscript.

Funding: This work was supported by Korea Institute of Energy Technology Evaluation and Planning (KETEP) grant funded by the Korea government (MOTIE) (No. 20192010107020, Development of hybrid adsorption chiller using unutilized heat source of low temperature).

Institutional Review Board Statement: Not applicable.

Informed Consent Statement: Not applicable.

Data Availability Statement: The data that support the findings of this study are available from the corresponding author upon reasonable request.

Conflicts of Interest: The authors declare no conflict of interest.

Abbreviations

The following abbreviations are used in this manuscript:

Symbol	Description and Unit
x, y	Cartesian coordinates [m]
u	horizontal component of nanofluid velocity [m/s]

u_p	x component of dust particles velocity (m/s)
v_p	y component of dust particles velocity (m/s)
T	temperature of the nanofluid (K)
T_p	temperature of the dust particles (K)
ϕ_d	volume fraction of dust particles
ϕ	volume fraction of nanoparticles
μ_{nf}	dynamic viscosity of nanofluid (m^2/s)
ρ_{nf}	density of nanofluid (kg/m^3)
K	Stokes resistance
N	number density of nanoparticles
m	mass of nanoparticles (kg)
$(\rho c_p)_{nf}$	specific heat capacity of the nanofluid (m^2/s^2K)
σ	electrical conductivity ($A^2s^3/kg \cdot m^3$)
B_0	induced magnetic flux ($V \cdot s$)
τ_T	thermal equilibrium time of the dust particles
τ_v	Relaxation time of the dust particles
c_p	specific heat of the nanofluid (J/K)
c_m	specific heat of the dust particles (J/K)
k_1	porosity parameter

References

- Mustafa, M.; Khan, J.A.; Hayat, T.; Alsaedi, A. Simulations for Maxwell fluid flow past a convectively heated exponentially stretching sheet with nanoparticles. *AIP Adv.* **2015**, *5*, 037133. <https://doi.org/10.1063/1.4916364>.
- Jamshed, W.; Eid, M.R.; Nasir, N.A.A.M.; Nisar, K.S.; Aziz, A.; Shahzad, F.; Shukla, A. Thermal examination of renewable solar energy in parabolic trough solar collector utilizing Maxwell nanofluid: A noble case study. *Case Stud. Therm. Eng.* **2021**, *101258*. <https://doi.org/10.1016/j.csite.2021.101258>.
- Fetecau, C.; Vieru, D.; Abbas, T.; Ellahi, R. Analytical solutions of upper convected Maxwell fluid with exponential dependence of viscosity under the influence of pressure. *Mathematics* **2021**, *9*, 334. <https://doi.org/10.3390/math9040334>.
- Nadeem, S.; Khan, M.R.; Khan, A.U. MHD stagnation point flow of viscous nanofluid over a curved surface. *Phys. Scr.* **2019**, *94*, 115207. <https://doi.org/10.1088/1402-4896/ab1eb6>.
- Arif, M.; Kumam, P.; Khan, D.; Watthayu, W. Thermal performance of GO-MoS₂/engine oil as Maxwell hybrid nanofluid flow with heat transfer in oscillating vertical cylinder. *Case Stud. Therm. Eng.* **2021**, *101290*. <https://doi.org/10.1016/j.csite.2021.101290>.
- Khan, M.I.; Alzahrani, F. Nonlinear dissipative slip flow of Jeffrey nanomaterial towards a curved surface with entropy generation and activation energy. *Math. Comput. Simul.* **2021**, *185*, 47–61. <https://doi.org/10.1016/j.matcom.2020.12.004>.
- Khan, M.I.; Alzahrani, F.; Hobiny, A.; Ali, Z. Modeling of Cattaneo-Christov double diffusions (CCDD) in Williamson nanomaterial slip flow subject to porous medium. *J. Mater. Res. Technol.* **2020**, *9*, 6172–6177. <https://doi.org/10.1016/j.jmrt.2020.04.019>.
- Siddiqa, S.; Begum, N.; Hossain, M.A. Compressible dusty gas along a vertical wavy surface. *Appl. Math. Comput.* **2017**, *293*, 600–610. <https://doi.org/10.1016/j.amc.2016.08.037>.
- Hamilton, R.L.; Crosser, O.K. Thermal conductivity of heterogeneous two-component systems. *Ind. Eng. Chem. Fundam.* **1962**, *1*, 187–191. <https://doi.org/10.1021/i160003a005>.
- Dey, D.; Chutia, B. Dusty nanofluid flow with bioconvection past a vertical stretching surface. *J. King Saud Univ.-Eng. Sci.* **2020**. <https://doi.org/10.1016/j.jksues.2020.11.001>.
- Zhang, X.H.; Abidi, A.; Ahmed, A.E.S.; Khan, M.R.; El-Shorbagy, M.A.; Shutaywi, M.; Galal, A.M. MHD stagnation point flow of nanofluid over a curved stretching/shrinking surface subject to the influence of Joule heating and convective condition. *Case Stud. Therm. Eng.* **2021**, *26*, 101184. <https://doi.org/10.1016/j.csite.2021.101184>.
- Khan, M.I.; Alzahrani, F.; Hobiny, A.; Ali, Z. Fully developed second order velocity slip Darcy-Forchheimer flow by a variable thicked surface of disk with entropy generation. *Int. Commun. Heat Mass Transf.* **2020**, *117*, 104778. <https://doi.org/10.1016/j.icheatmasstransfer.2020.104778>.
- Krishna, M.V.; Ahamad, N.A.; Chamkha, A.J. Hall and ion slip impacts on unsteady MHD convective rotating flow of heat generating/absorbing second grade fluid. *Alex. Eng. J.* **2021**, *60*, 845–858. <https://doi.org/10.1016/j.aej.2020.10.013>.
- Li, Y.X.; Waqas, H.; Al-Khaled, K.; Khan, S.A.; Khan, M.I.; Khan, S.U.; Chu, Y.M. Simultaneous features of Wu's slip, nonlinear thermal radiation and activation energy in unsteady bio-convective flow of Maxwell nanofluid configured by a stretching cylinder. *Chin. J. Phys.* **2021**. <https://doi.org/10.1016/j.cjph.2021.07.033>.
- Mohammadein, S.A.; Raslan, K.; Abdel-Wahed, M.S.; Abedel-Aal, E.M. KKL-model of MHD CuO-nanofluid flow over a stagnation point stretching sheet with nonlinear thermal radiation and suction/injection. *Results Phys.* **2018**, *10*, 194–199. <https://doi.org/10.1016/j.rinp.2018.05.032>.

16. Zainal, N.A.; Nazar, R.; Naganthran, K.; Pop, I. MHD mixed convection stagnation point flow of a hybrid nanofluid past a vertical flat plate with convective boundary condition. *Chin. J. Phys.* **2020**, *66*, 630–644. <https://doi.org/10.1016/j.cjph.2020.03.022>.
17. Eastman, J.A.; Choi, U.S.; Li, S.; Thompson, L.J.; Lee, S. Enhanced thermal conductivity through the development of nanofluids. *Mrs Online Proc. Libr. (OPL)* **1996**, *457*, 3–11. <https://doi.org/10.1557/PROC-457-3>.
18. Khan, M.R.; Pan, K.; Khan, A.U.; Ullah, N. (2020). Comparative study on heat transfer in CNTs-water nanofluid over a curved surface. *Int. Commun. Heat Mass Transf.* **2020**, *116*, 104707. <https://doi.org/10.1016/j.icheatmasstransfer.2020.104707>
19. Ishak, A.; Nazar, R.; Pop, I. Dual solutions in mixed convection boundary layer flow of micropolar fluids. *Commun. Nonlinear Sci. Numer. Simul.* **2009**, *14*, 1324–1333. <https://doi.org/10.1016/j.cnsns.2008.01.017>.
20. Ghosh, N.C.; Ghosh, B.C.; Gorla, R.S.R. Hydromagnetic flow of a dusty viscoelastic Maxwell fluid through a rectangular channel. *Int. J. Fluid Mech. Res.* **2007**, *34*. doi:10.1615/InterJFluidMechRes.v34.i1.20.
21. Ahmed, S.F.; Hafez, M.G.; Chu, Y.M. Conversion of energy equation for fiber suspensions in dusty fluid turbulent flow. *Results Phys.* **2020**, *19*, 103341. <https://doi.org/10.1016/j.rinp.2020.103341>.
22. Damseh, R.A. Thermal boundary layer on an exponentially stretching continuous surface in the presence of magnetic field effect. *Int. J. Appl. Mech. Eng.* **2006**, *11*, 289–299.
23. Naramgari, S.; Sulochana, C. MHD flow of dusty nanofluid over a stretching surface with volume fraction of dust particles. *Ain Shams Eng. J.* **2016**, *7*, 709–716. <https://doi.org/10.1016/j.asej.2015.05.015>.
24. Bhattacharyya, K.; Pop, I. MHD boundary layer flow due to an exponentially shrinking sheet. *Magneto hydrodynamics* **2011**, *47*, 337–344. <http://doi.org/10.22364/mhd>.
25. Ellahi, R.; Zeeshan, A.; Hassan, M. Particle shape effects on Marangoni convection boundary layer flow of a nanofluid. *Int. J. Numer. Methods Heat Fluid Flow* **2016**, *26*, 2160–2174. <https://doi.org/10.1108/HFF-11-2014-0348>.
26. Saidu, I.; Waziri, M.M.; Roko, A.; Musa, H. MHD effects on convective flow of dusty viscous fluid with volume fraction of dust particles. *J. Eng. Appl. Sci.* **2010**, *5*, 86–91.
27. Akbar, N.S.; Nadeem, S.; Haq, R.U.; Khan, Z.H. Numerical solutions of magnetohydrodynamic boundary layer flow of tangent hyperbolic fluid towards a stretching sheet. *Indian J. Phys.* **2013**, *87*, 1121–1124. <https://doi.org/10.1007/s12648-013-0339-8>.
28. Wahid, N.S.; Arifin, N.M.; Khashi'ie, N.S.; Pop, I. Marangoni hybrid nanofluid flow over a permeable infinite disk embedded in a porous medium. *Int. Commun. Heat Mass Transf.* **2021**, *126*, 105421. <https://doi.org/10.1016/j.icheatmasstransfer.2021.105421>.
29. Hossain, M.A.; Roy, N.C.; Siddiqua, S. Unsteady mixed convection dusty fluid flow past a vertical wedge due to small fluctuation in free stream and surface temperature. *Appl. Math. Comput.* **2017**, *293*, 480–492. <https://doi.org/10.1016/j.amc.2016.08.048>.
30. Sandeep, N.; Sugunamma, V.; Mohankrishna, P. Effects of radiation on an unsteady natural convective flow of a EG-Nimonic 80a nanofluid past an infinite vertical plate. *Adv. Phys. Theor. Appl.* **2013**, *23*, 36–43. <https://doi.org/10.1142/S179329201350001X>.
31. Mandal, S.; Shit, G.C. Entropy analysis on unsteady MHD biviscosity nanofluid flow with convective heat transfer in a permeable radiative stretchable rotating disk. *Chin. J. Phys.* **2021**, <https://doi.org/10.1016/j.cjph.2021.07.036>.
32. Daniel, Y.S.; Aziz, Z.A.; Ismail, Z.; Salah, F. Thermal radiation on unsteady electrical MHD flow of nanofluid over stretching sheet with chemical reaction. *J. King Saud Univ.-Sci.* **2019**, *31*, 804–812. <https://doi.org/10.1016/j.jksus.2017.10.002>.
33. Ghasemi, S.E.; Hatami, M. Solar radiation effects on MHD stagnation point flow and heat transfer of a nanofluid over a stretching sheet. *Case Stud. Therm. Eng.* **2021**, *25*, 100898. <https://doi.org/10.1016/j.csite.2021.100898>.
34. Sandeep, N.; Saleem, S. MHD flow and heat transfer of a dusty nanofluid over a stretching surface in a porous medium. *Jordan J. Civ. Eng.* **2017**, *11*, 149–164.
35. Sheikholeslami, M.; Rokni, H.B. Nanofluid two phase model analysis in existence of induced magnetic field. *Int. J. Heat Mass Transf.* **2017**, *107*, 288–299. <https://doi.org/10.1016/j.ijheatmasstransfer.2016.10.130>.
36. Buongiorno, J. Convective transport in nanofluids. *J. Heat Transfer* **2006**, 240–250. <https://doi.org/10.1115/1.2150834>.
37. Nield, D.A.; Kuznetsov, A.V. The Cheng–Minkowycz problem for natural convective boundary-layer flow in a porous medium saturated by a nanofluid. *Int. J. Heat Mass Transf.* **2009**, *52*, 5792–5795. <https://doi.org/10.1016/j.ijheatmasstransfer.2009.07.024>.
38. Batchelor, C.K.; Batchelor, G.K. *An Introduction to Fluid Dynamics*; Cambridge University Press: Cambridge, UK, 2000.
39. Ling, J.X.; Dybbs, A. *Forced Convection over a Flat Plate Submersed in a Porous Medium: Variable Viscosity Case (No. CONF-871234-)*; American Society of Mechanical Engineers: New York, NY, USA, 1987.
40. McTaggart, C.L. Convection driven by concentration-and temperature-dependent surface tension. *J. Fluid Mech.* **1983**, *134*, 301–310. <https://doi.org/10.1017/S0022112083003377>.
41. Mishra, S.R.; Sun, T.C.; Rout, B.C.; Khan, M.I.; Alaoui, M.K.; Khan, S.U. Control of dusty nanofluid due to the interaction on dust particles in a conducting medium: Numerical investigation. *Alex. Eng. J.* **2021**. <https://doi.org/10.1016/j.aej.2021.07.026>.
42. Mahanthesh, B.; Gireesha, B.J.; PrasannaKumara, B.C.; Shashikumar, N.S. Marangoni convection radiative flow of dusty nanofluid with exponential space dependent heat source. *Nucl. Eng. Technol.* **2017**, *49*, 1660–1668. <https://doi.org/10.1016/j.net.2017.08.015>.
43. Kannan, A.S.; Mark, A.; Maggiolo, D.; Sardina, G.; Sasic, S.; Ström, H. A hydrodynamic basis for off-axis Brownian diffusion under intermediate confinements in micro-channels. *Int. J. Multiph. Flow* **2021**, 103772. <https://doi.org/10.1016/j.ijmultiphaseflow.2021.103772>.
44. Gabbasov, R.; Yurenya, A.; Nikitin, A.; Cherepanov, V.; Polikarpov, M.; Chuev, M.; Panchenko, V. Study of Brownian motion of magnetic nanoparticles in viscous media by Mössbauer spectroscopy. *J. Magn. Magn. Mater.* **2019**, *475*, 146–151. <https://doi.org/10.1016/j.jmmm.2018.11.044>.
45. Heyse, A.; Kraume, M.; Drews, A. The impact of lipases on the rheological behavior of colloidal silica nanoparticle stabilized Pickering emulsions for biocatalytical applications. *Colloids Surf. Biointerfaces* **2020**, *185*, 110580.

46. Riedl, J.C.; Sarkar, M.; Fiuza, T.; Cousin, F.; Depeyrot, J.; DUBOIS, E.; Peyre, V. Design of long-term stable concentrated colloidal dispersions in ionic liquids up to 473 K. *J. Colloid Interface Sci.* 2021. <https://doi.org/10.1016/j.jcis.2021.08.017>.
47. Salamon, P.; Geng, Y.; Eremin, A.; Stannarius, R.; Klein, S.; Börzsönyi, T. Rheological and flow birefringence studies of rod-shaped pigment nanoparticle dispersions. *J. Mol. Liq.* **2020**, *313*, 113401. <https://doi.org/10.1016/j.molliq.2020.113401>.
48. Ma, M.Y.; Zhai, Y.L.; Li, Z.H.; Yao, P.T.; Wang, H. Particle size-dependent rheological behavior and mechanism of Al₂O₃-Cu/W hybrid nanofluids. *J. Mol. Liq.* **2021**, *335*, 116297. <https://doi.org/10.1016/j.molliq.2021.116297>.